Lecture 9

Mechanisms and toy models of the glacial cycles

Eli Tziperman

Given the above climate feedbacks as our ingredients for making glacial theories, we now describe some of the physical mechanisms and models proposed for explaining the main features of the glacial cycles. As done throughout these lectures, we concentrate on conceptual (toy) models that attempt to explore the role of a limited number of feedbacks at a time.

9.9 Glacial mechanisms based on basic physical feedbacks

9.9.1 Temperature-precipitation feedback

(Ghil [14]) The ice albedo feedback, relating rate of change of the temperature (T) to the albedo and to the land ice volume (V_{ice}), may be written as

$$\frac{dT}{dt} \quad \propto \quad -albedo \propto -V_{ice}.$$

Together with the temperature-precipitation (p) feedback

$$\frac{dV_{ice}}{dT} \propto p \propto T$$

the two feedbacks may be combined into a single equation that has an oscillatory solution

$$\frac{d^2T}{dt^2} \propto -T.$$

However, it turns out the time scale of these linear oscillations is much too short (10,000 years). In addition, this linear mechanism cannot account for the saw-tooth structure of the oscillations, and some nonlinearity must be included.

9.9.2 Glacial oscillations based on isostatic adjustment: the Load-accumulation feedback

(Ghil [14]) Assume that higher elevation of the ice sheet surface results in colder ice-sheet surface temperature, therefore in less ablation, and therefore in *more* net accumulation (i.e. opposite of the elevation-desert effect). As the ice volume increases, the ice sheet sinks into the bedrock, moving more of the the glacier surface area into an elevation of less accumulation/ more ablation (or equivalently, moving the equilibrium line poleward). This results in a negative feedback between ice volume and net accumulation rate

$$\frac{dp}{dt} \propto -V_{ice}$$

which, together with the simple mass balance equation

$$\frac{dV_{ice}}{dT} \propto p$$

again results in an oscillatory equation. The oscillation time scale is too short again due to the too short time scale of the isostatic adjustment. Again, this linear mechanism cannot account for the saw-tooth structure of the oscillations, and some nonlinearity must be included. A more sophisticated version of this mechanism, including calving, Milankovitch, and a nonlinear isostatic adjustment parameterization will be presented below.

9.9.3 Milankovitch forcing

Orbital/ incoming solar variations seem natural candidates for a glacial theory given their time scale and potential climatic effects. Indeed, as reviewed by Paillard ([41], Fig. 53) such theories have been proposed as early as the nineteenth century. In fact, it turns out that Milankovitch forcing by itself is unlikely to be able to explain the observed characteristics of the glacial cycles, although it does seem to play a significant, even if secondary, role in the cycles dynamics.

Milankovitch seems to have been the first to understand that the solar radiation during the summer season is the critical climatic factor, as cold summers allow the survival of new snow cover from winter season (section 8.8.5 above). He also accurately calculated the time variations of the different orbital parameters. However, the dominant effect of the precession and obliquity on the summer radiation leads to a prediction of glacial cycle frequency of 19, 23 and 41 kyr periods, not in agreement with the dominant 100 kyr climatic signal (Fig. 56).
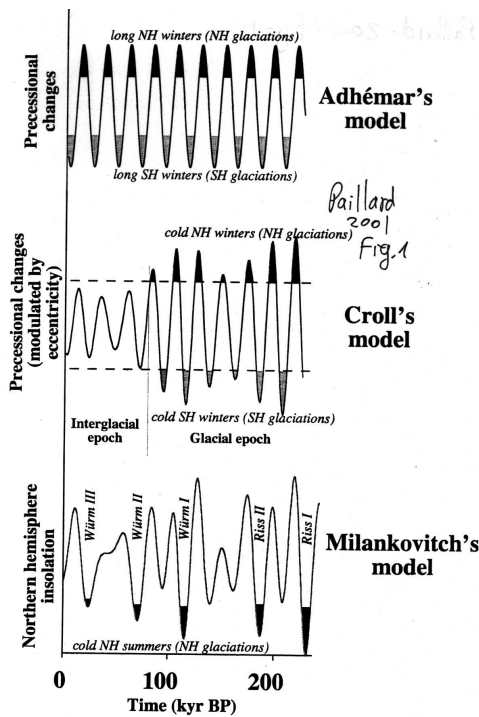

Figure 53: Three historical glacial theories based on orbital variations (Fig. 1 from Paillard [41])

The role of Milankovitch forcing is easily quantified using some simple model equations, and various versions of such toy models have been proposed over the years (Calder, [6]; Imbrie and Imbrie [26]; Held [22]; see nice review by Paillard [41]). The simplest equation for the global ice volume in terms of Milankovitch forcing would be something like [6];

$$\frac{dV_{ice}}{dt} = -k(i - i_0) \tag{36}$$

where i is the insolation, i_o is the mean insolation, and where the proportionality constant k may have different values for melting $(i > i_0)$ and for accumulation $(i < i_0)$. While integrating this equation, one may also impose a condition that $V_{ice} > 0$. However, the fit to observations is rather poor... (Fig. 54, from Paillard [41], Fig. 9)
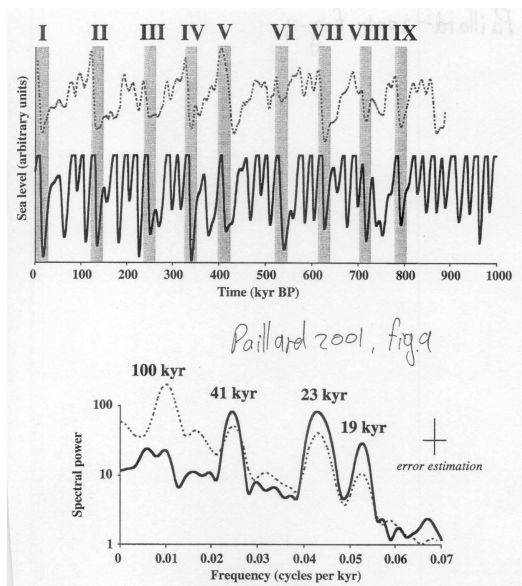
112

Figure 54: Results of the glacial cycle model of equation 36 (Paillard 2001, Fig. 9)

Next, Imbrie and Imbrie [26] use (nondimensional)

$$\frac{dV_{ice}}{dt} = (i - V_{ice})/\tau \tag{37}$$

again with different τ for melting ($V_{ice} > i$) and accumulation. This model assumes a simple relaxation of the ice volume to the summer radiation, with the relaxation time scale given by τ. The results show a small peak at 100 kyr, and a larger one at 400 kyr, which is clearly still not a satisfactory result [41].

Analysis of the proxy records shows that the precession (19 & 23 kyr) and Obliquity (41 kyr) bands are likely to be linearly forced by Milankovitch forcing, but that the 100 kyr band is not likely to be directly and linearly forced by Milankovitch variations because Milankovitch forcing is much too weak at the 100 kyr period (Figs. 55, 56). Could the 100 kyr signal be a linear resonant response to the very weak Milankovitch forcing? Again not likely because there does not seem to be any linear time scale of the order of 100 kyr in the climate system that may be excited to produce the observed response. In order to obtain a time scale of 100 kyr, a different mechanism is clearly needed, most likely a nonlinear one. Various nonlinear feedbacks were indeed tried as will be discussed below.

Given the failure of the above simple linear models to explain the 100 kyr peak using Milankovitch forcing, Le-Treut and Ghil have tried to explain this peak as being due to nonlinear frequency transfer from Milankovitch frequencies to the 100 kyr period ([33], [14]). To do this, they combined the temperature-precipitation feedback and ice-albedo feedback which were shown above to produce glacial oscillations, using a few refinements that produced nonlinear self-sustained oscillations with a time scale of some 7-10 kyr. The interaction of these nonlinear oscillations with the Milankovitch forcing results in a 100 kyr time scale. Let us begin the description of this mechanism by briefly describing the nonlinear oscillator model. Let the ratio of the ice sheet's accumulation area (a) and ablation area (a') be given by $\varepsilon(T) = a/a'$. This ratio varies nonlinearly as a function of the temperature (Fig. 57), and represents the effect of the temperature on the ablation/ accumulation according to the temperature precipitation feedback. In addition, the ocean albedo (α_{oc}) is also assumed to vary nonlinearly with the temperature (Fig. 57), while the land albedo is just linear in the land ice area.
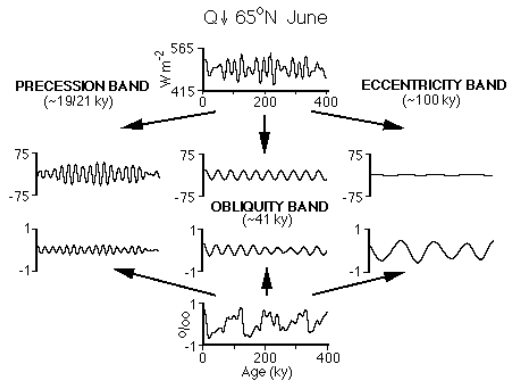
113

Figure 55: Imbrie et al; decomposition of climate record into Milankovitch spectral bands
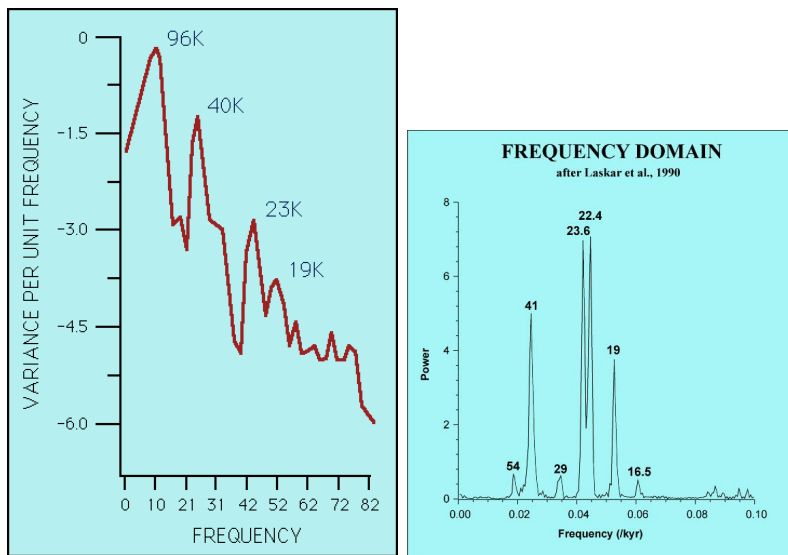

Figure 56: Spectra of Milankovitch (right) and proxy records (left), showing why Milankovitch is not the likely explanation for the 100 kyr time scale
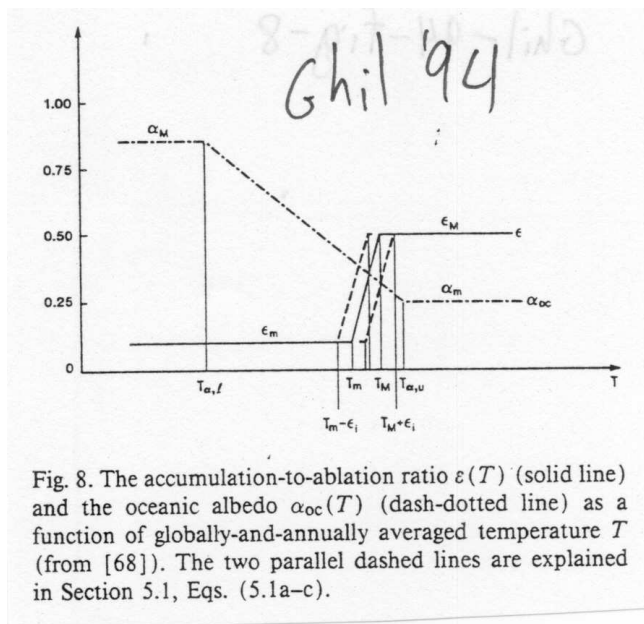
Fig. 8. The accumulation-to-ablation ratio $\varepsilon(T)$ (solid line) and the oceanic albedo $\alpha_{oc}(T)$ (dash-dotted line) as a function of globally-and-annually averaged temperature T (from [68]). The two parallel dashed lines are explained in Section 5.1, Eqs. (5.1a–c).

Figure 57: Sea ice albedo and accumulation factor as function of temperature (Fig. 8 from Ghil [14])

The temperature equation (roughly equivalent to the over simplified $dT/dt \propto -V_{ice}$ above) includes the effects of incoming solar radiation Q, land and ocean albedos and a linearized outgoing long wave radiation term

$$c_T \frac{dT}{dt} = Q\{1 - [\gamma\alpha_{land}(\ell) + (1-\gamma)\alpha_{oc}(T)]\} - \kappa(T - T_k).$$

The equation for the meridional extent of the land ice sheet, ℓ, is based on the temperature-precipitation feedback and has the form (roughly equivalent to the over simplified $dV_{ice}/dt \propto T$ above)

$$c_L \frac{d\ell}{dt} = \ell^{-1/2}\{[1 + \varepsilon(T)]\ell_T(T,\ell) - \ell\}$$

where c_L is some relaxation constant, and $\ell_T(T,\ell)$ represents the location of the boundary between the accumulation and ablation zones on the ice sheet.

As mentioned above, this model results in a self-sustained oscillation with a period that is quite robust around 6-7 kyr. Next, Milankovitch forcing is included by making the ratio of ablation to accumulation areas a function of temperatures $T_m(t), T_M(t)$ which are, in turn, a function of the Milankovitch radiation: $\varepsilon = \varepsilon(T, T_m(t), T_M(t))$, (see again Fig. 57 for an explanation of the physical role of $T_m(t), T_M(t)$). The Milankovitch forcing appears not as a free forcing term on the rhs, but as a parametric forcing term multiplying other terms in the equations. When the model is first forced with a single frequency f_j, one sees the response, instead of at the original (non-Milankovitch) frequency $f_0 \approx 7kyr^{-1}$, showing up at integer multiples of the forcing frequency f_j, so that the system oscillates at frequencies kf_j, with integer k, especially such that kf_j is close to the original unforced frequency f_0. This is again, as discussed in the case of El Nino, a nonlinear resonant response. When the model is forced with two Milankovitch frequencies the response is seen at "combination tones" of the form $k_1f_1 + k_2f_2$. This could be with a "sum tone" $k_1k_2 > 0$ or a "difference tone" $k_1k_2 < 0$. For sufficiently strong Milankovitch

115

forcing, one gets a chaotic response with many different combination tones. In particular, the dominant response tone turns out to be at a frequency

$$\frac{1}{109}kyr^{-1} = f_1 - f_2 = \frac{1}{19}kyr^{-1} - \frac{1}{23}kyr^{-1}$$

So that we obtain an explanation of the 100 kyr as a nonlinear response to the two major precession frequencies! While the spectrum of this response is quite satisfactory, with the 109 kyr frequency dominating the 41, 23 & 19 kyr frequencies (Fig. 58), the detailed characteristic features of the time series, are perhaps not completely satisfactory (Fig. 59) when compared to the proxy (in particular ice core) records.
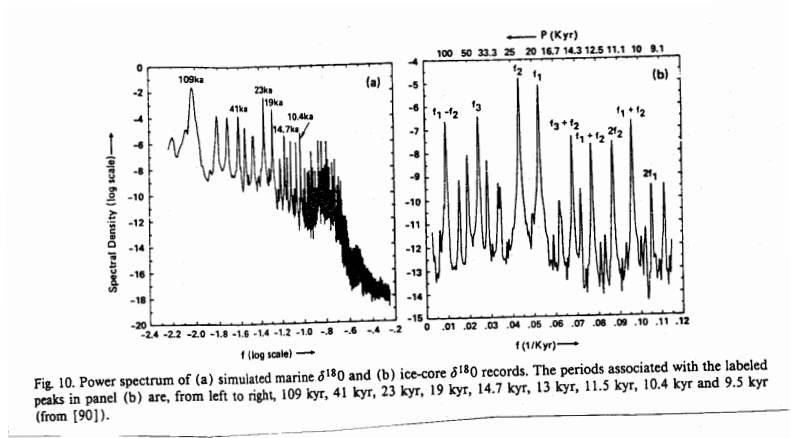

Fig. 10. Power spectrum of (a) simulated marine $\delta^{18}O$ and (b) ice-core $\delta^{18}O$ records. The periods associated with the labeled peaks in panel (b) are, from left to right, 109 kyr, 41 kyr, 23 kyr, 19 kyr, 14.7 kyr, 13 kyr, 11.5 kyr, 10.4 kyr and 9.5 kyr (from [90]).

Figure 58: Spectrum of chaotic model regime, showing a 100 kyr peak (Fig. 10 from Ghil [14])

Fig. 11. Model-simulated marine $\delta^{18}O$ record; its power spectrum appears in Fig. 10a (from [90]).
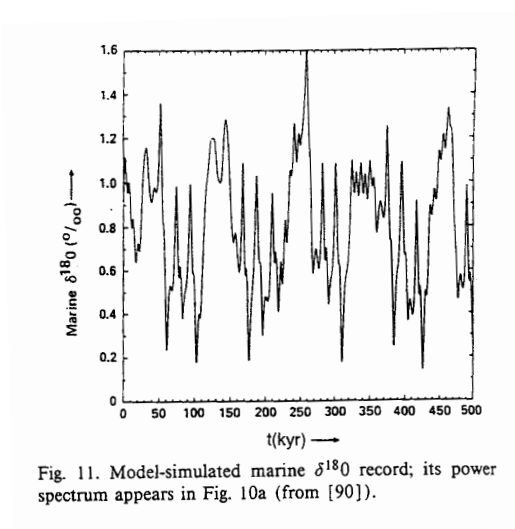
Figure 59: Time series of the same model as in the previous figure [Fig. 11, Ghil [14]]

However, additional efforts to use combination tones of Milankovitch frequency to explain the 100 kyr peak

116

continue, and Rial [51], for example, recently suggested a 'simple' explanation for the glacial cycle time scale based on the following combination tones . . .

$$\frac{1}{107} kyr^{-1} = \frac{1}{95} kyr^{-1} - \frac{1}{826} kyr^{-1}.$$

Given the need to use some nonlinear mechanism together with the Milankovitch signal to explain the 100 kyr period, Paillard [40] suggested that the mechanism might be jumps between steady states of the climate system, driven by Milankovitch forcing. Such jumps between different steady states imply an important nonlinearity in the climate system that allows the existence of such multiple steady states and the jumping between them (both could not exist in a linear system). Paillard argues for separating the ice volume and global temperature and allowing them to be independent (yet coupled) degrees of freedom. He also assumes the glacial cycles to be due to jumps of the climate system between three different modes: i (interglacial), g (mild glacial), and G (full Glacial). Rules are *specified* for the transition between these modes

- $i \rightarrow g$ (glaciation begins) occurs when the insolation decreases below a threshold i_0.

- $g \rightarrow G$ (glaciation approaching its maximum) occurs when the ice volume increases above some threshold value v_{max}.

- $G \rightarrow i$ (deglaciation) occurs when the insolation increases above some threshold i_1, where $i_1 > i_0$.

The equation determining the ice volume evolution at each "mode" or "regime" (indicated by the index R which can take the values i, g, G) is

$$\frac{dV_{ice}}{dt} = -\frac{V_R - V}{\tau_R} - \frac{F}{\tau_F}$$

where the ice volume to which the system is restored at each mode is different

$$V_i = 0; \qquad V_g, V_G = 1$$

and where F is the Milankovitch summer radiation. This model may be seen as an extension of the Imbrie and Imbrie model to a multiple-regimes scenario. The results of this model fit the SPECMAP record very nicely (Fig. 60), although perhaps this is not completely surprising given the quite a few available tuning parameters (V_R, τ_R, $R = \{i, g, G\}$).

This model does not provide us with an explanation of what the actual physical mechanism is, what component of the climate system is responsible for the thresholds/ multiple modes, why are the relaxation times τ_R different for each regime and what determines them, etc.

This simple model does indicate that thresholds and rapid transition processes are important. It also demonstrates that one can get a good fit to observations due to a phase locking to Milankovitch forcing, as also shown by Saltzman's models and discussed next. This is the same phenomenon discussed in the context of El Nino and seen in Fig. 28: any nonlinear oscillator with a time scale of roughly 100 kyr that is constructed based on some internal variability mechanism yet is driven by Milankovitch radiation is likely to be phase locked to the Milankovitch forcing. A phased locked glacial oscillation is shown for example in Fig. 61 from the work of Gildor and Tziperman [16] discussed below. Thus it seems that while the 100 kyr Milankovitch forcing plays no significant role in glacial dynamics, the phase locking to 19, 23 and 41 kyr accounts for the observed phase of the oscillations; that is, for the observed timing of deglaciations. Note that because the Milankovitch forcing is not periodic but rather quasi-periodic and therefore somewhat irregular in time, the locking of the glacial cycle to the Milankovitch forcing also induce somewhat irregular glacial cycles. In particular, this explains the variability of the glacial period around 100 kyr between different glaciations. It seems, therefore, that the irregularity of the glacial cycles is likely due to the quasi-periodic nature of Milankovitch forcing, rather than an indication that the glacial dynamics themselves are chaotic.
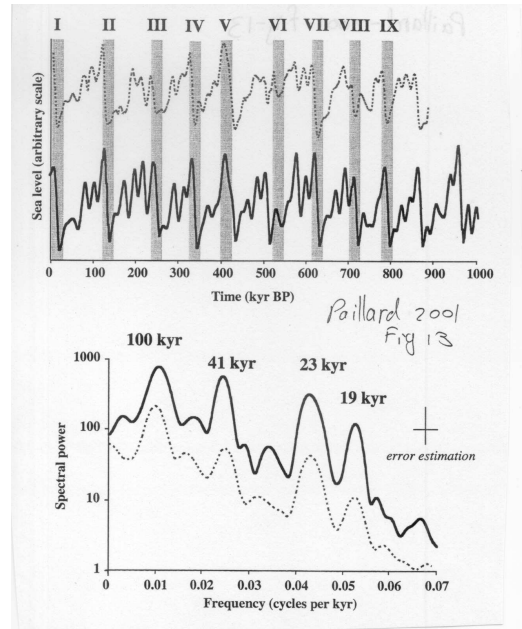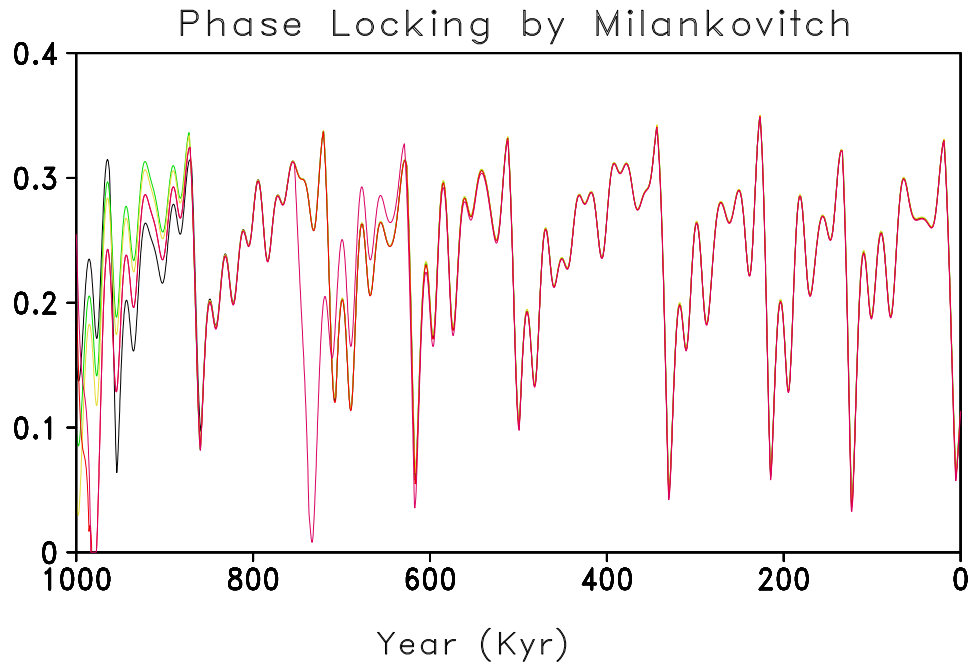
Figure 60: Fig. 13 from Paillard 2001

Figure 61: Phase locking to Milankovitch: land ice volume as function of time for six different model runs having different initial conditions. All runs converge fairly rapidly to a single time series as they are all locked to the phase imposed by specified Milankovitch forcing (Gildor and Tziperman, [16]).

9.9.4 Glacial oscillations based on isostatic adjustment + Milankovitch + Calving

Another effort to obtain a 100 kyr glacial cycle from Milankovitch forcing is based on a nonlinear version of the load accumulation linear mechanism discussed in section 9.9.2 and based on the isostatic adjustment. To do that, the nonlinear dynamics of ice sheet flow is added, as well as a calving parameterization (Pollard, [48, 49]). The Milankovitch forcing is specified, similarly to [33], by making the equilibrium line location vary with the Milankovitch radiation at, say, 55N:

$$E(y, t) = E_0 + E_1 y + E_2 Q(55°)$$

The results are shown in Fig. 62 and the fit to the observed global ice volume is not too bad (lowest panel of that Figure). It turns out, however, that when trying to formulate a model that uses isostatic adjustment to obtain the 100 kyr glacial cycles, one needs to use too long time scale for the isostatic adjustment (10 kyr instead of the more realistic 3 kyr) in order to obtain a good fit to observations. Furthermore, one needs to add quite a few additional feedbacks such as the topography of the crust (which enters the isostatic adjustment parameterization discussed above, and affects the initial ground height, which is important for the source-sink function for the glacier mass balance), and a calving parameterization. Overall, it seems that too many different feedbacks are needed (Fig. 62) and that this mechanism is not as simple and clean as one would have hoped given the seemingly simple structure of the glacial signal.
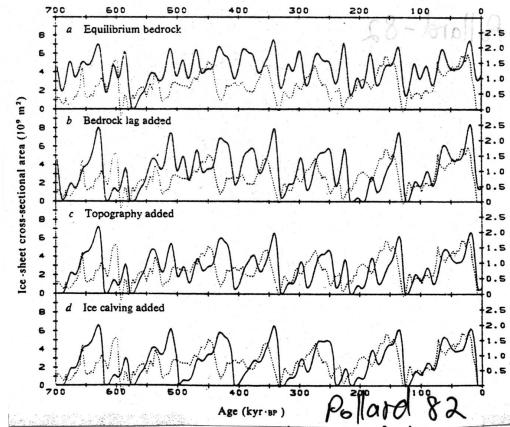

Figure 62: Fit of a glacial model results to observations. The complexity of the feedbacks used increases from the upper panel toward the lower one. See text for details. (Fig. 1 from Pollard [48]).

9.9.5 Stochastic resonance

An elegant mechanism that combines 100 kyr Milankovitch forcing with stochastic noise forcing has been suggested by Benzi, Parisi, Sutera and Vulpiani [3]. This mechanism is not likely to be a correct explanation for the glacial dynamics, yet the physical idea seems to have found many interesting applications outside the research area of climate dynamics, so it is worth examining. Consider a simple model of the climate system that is governed by a zero-dimensional global energy balance model equation such as

$$\frac{dT}{dt} = R_{in}(T) - R_{out}(T) + \sigma\eta(t) = F(T) + \sigma\eta(t) = -\frac{\partial\Phi}{\partial T} + \sigma\eta(t)$$

119

where $R_{in}(T)$ and $R_{out}(T)$ are the incoming and outgoing radiation terms and $\sigma\eta(t)$ is a white noise term due to internal noise of the climate system (e.g. weather). The potential function $\Phi(T)$ chosen such that it has two minima where $F = -\partial\Phi/\partial T = 0$ at the two temperatures T_1, T_2, which represent stable equilibria corresponding to glacial and interglacial conditions) separated by a maximum (an unstable equilibrium point). More explicitly, the potential Φ is given by

$$F(T) = -\frac{\partial\Phi}{\partial T} = \frac{\varepsilon(T)}{C} \times \frac{\mu(t)}{1 + \beta(1 - T/T_1)(1 - T/T_2)(1 - T/T_3)},$$

with

$$\mu(T) = 1 + 0.0005\cos(\omega t); \qquad \omega = 2\pi/10^5 years$$

representing the 100 kyr orbital forcing frequency. The system is therefore driven by both slow small amplitude oscillations in the potential due to Milankovitch forcing, $\mu(t)$, and by the white noise $\sigma\eta(t)$. To see the potential function, try in Matlab:

```
for i=1:40; f(i)=1.0/(1+ 0.1*(1.0-i/10.1)*(1.0-i/20.1)*(1.0-i/30.1));end; plot(f)
g(1)=0; for i=1:40; g(i+1)=g(i)+f(i)-1; end; plot(g)
```

The effect of $\mu(t)$ is to lower and raise the two minima of the potential with respect to the middle barrier, as shown in Fig. 63. In the absence of the white noise, the system undergoes small oscillations about one of the stable steady states due to the oscillations in $\mu(t)$. Similarly, in the absence of the periodic changes to the potential, the white noise term induces variability depending on its amplitude: if the white noise is not sufficiently strong, there would be no transition in this case between the minima, but only small stochastic variability about one of the minima; if the stochastic forcing is strong enough, there is some probability of jumping between the stable equilibria, but with no preferred periodicity.

Now, suppose that both the stochastic white noise forcing and slow 100 kyr variations act together. Assume further that the white noise by itself is not sufficiently strong to induce transitions between the equilibria. Such transitions may still be possible because of the slow variations in the potential induced by $\mu(t)$: when these slow variations lower the potential barrier as in panel A of Fig. 63, the white noise may be sufficiently strong to cause a transition from the left to the right potential wells. The next transition will be possible when the potential barrier is reduced for the potential well on the right (panel C). As a result of this combination of white noise and slow modulations of the potential well, the system will produce a preferred periodicity at 10^5 years and a corresponding spectral peak at that frequency. This is termed "stochastic resonance" because a too weak noise wont induce transitions, and too strong noise will not show the preferred periodicity (it the stochastic forcing would then be able to induce transitions regardless of the slow oscillations in the potential). That an optimal noise level is needed, justifies the use of the term "resonance".

Because this mechanism relies on the 100 kyr Milankovitch signal which is very weak climatically, and because the resulting time series does not have the saw tooth structure, the stochastic resonance is not a likely candidate for the 100 kyr glacial cycle mechanism. Furthermore, the mechanism is formulated in very general terms, avoiding the issues of what is the source of the white noise, which specific climate component is responsible for the double well potential (this needs to be some nonlinearly behaving component that allows for multiple minima), etc. This mechanism therefore does not make specific physical predictions that may be falsified beyond the shape of the time series which, as mentioned above, is already inconsistent with the observed one.

9.9.6 "Earth-system" models (Saltzman et al.)

In a series of works, Saltzman and co-workers have used various models that are all based on a similar approach: write a set of three ordinary differential equations for three prognostic climate variables; include various linear and
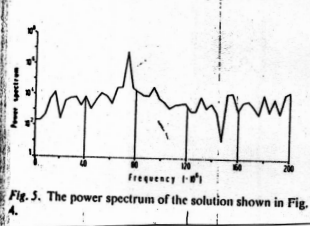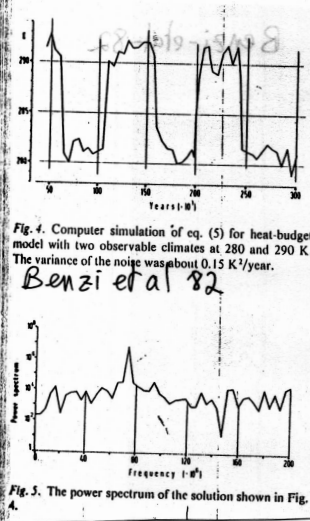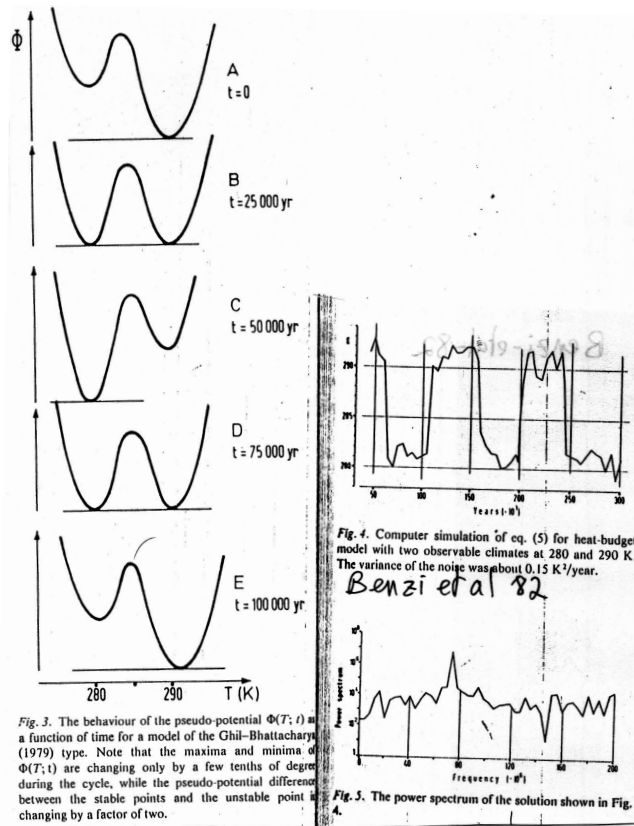
Fig. 3. The behaviour of the pseudo-potential $\Phi(T;t)$ as a function of time for a model of the Ghil–Bhattacharya (1979) type. Note that the maxima and minima of $\Phi(T;t)$ are changing only by a few tenths of degree during the cycle, while the pseudo-potential difference between the stable points and the unstable point is changing by a factor of two.

Fig. 4. Computer simulation of eq. (5) for heat-budget model with two observable climates at 280 and 290 K. The variance of the noise was about 0.15 K²/year.

Benzi et al 82

Fig. 5. The power spectrum of the solution shown in Fig. 4.

Figure 63: Figs. from Benzi et al showing potential function and time series of transitions

121

nonlinear feedbacks between the three variables; while allowing the physical assumptions and prognostic variables that vary somewhat from work to work, always assume that: (1) the system should have a free (self sustained) oscillation of roughly 100,000 year period; (2) Milankovitch forcing provides the precise phase of the oscillation via nonlinear phase locking. In many of these works CO_2 is assumed to be a key variable that maintains the 100 kyr oscillation which will not exist without it. The set of feedbacks used for example by Saltzman and Sutera [52] is shown in Fig. 64.
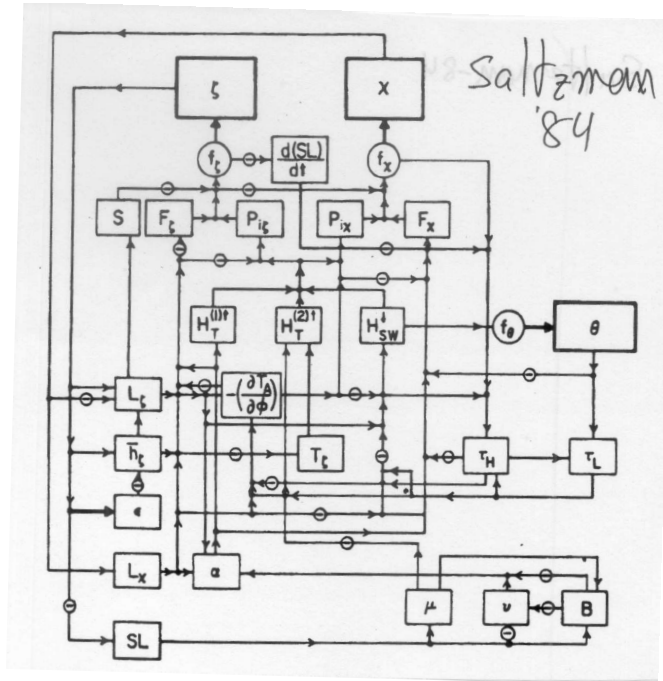

Figure 64: A set of feedbacks included in a simple climate model... (Fig. 3 from Saltzman and Sutera [52]).

Let us consider two examples of feedback loops used in this approach and see how they are converted into a mathematical form. In the following, $-\oplus\rightarrow$ and $-\ominus\rightarrow$ correspond to a positive and negative feedbacks, correspondingly:

1. (#2 in Saltzman and Sutera [52], p 740): Increased marine-based ice volume $-\oplus\rightarrow$ increased marine ice area and albedo $-\ominus\rightarrow$ decreased temperature and therefore decreased source term for land glacier mass balance (via temperature-precipitation feedback) $-\oplus\rightarrow$ decreased land ice volume. Bottom line, it's a negative feedback, add a term to the equation for the land ice volume that depends on the marine ice volume

$$\frac{dV_{land\,ice}}{dt} = \dots - C_1 \times [\text{marine based ice}]$$

2. CO_2 feedback (#11 in Saltzman and Sutera [52], p 741): increased land ice volume $-\ominus\rightarrow$ reduced sea level $-\oplus\rightarrow$ reduced atmospheric CO_2 (why...?) $-\ominus\rightarrow$ increased outgoing long-wave radiation increased accumulation over land glaciers $-\ominus\rightarrow$ increased land ice volume. Bottom line: a positive feedback

$$\frac{dV_{land\,ice}}{dt} = \dots + C_2 \times V_{land\,ice}$$

122

The resulting set of nondimensional equations (from Saltzman [53]) is of the form

$$\frac{dX}{dt} = -\alpha_1 Y - \alpha_2 Z - \alpha_3 Y^2$$

$$\frac{dY}{dt} = -\beta_0 X + \beta_1 Y + \beta_2 Z - (X^2 + 0.004Y^2)Y + F_Y$$

$$\frac{dZ}{dt} = X - \gamma_2 Z$$

where in this particular case X, Y and Z are the ice mass, deep ocean temperature and atmospheric carbon dioxide. The fit to the global ice volume proxy curves in these models is normally quite impressive (Fig. 65). This is not necessarily a surprise, as the quite a few coefficients in the above three equations are chosen to optimize this fit.
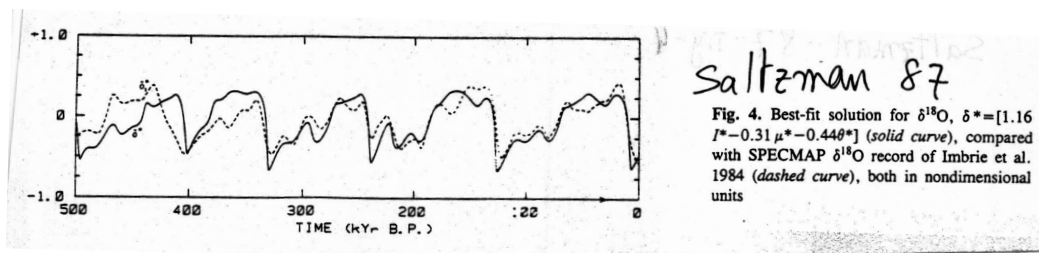

Figure 65: Fit of model to global ice volume proxy data. Fig. 4 from Saltzman [53]

Of course, one needs to be very careful in trying too hard to fit model results to proxy data, as shown by the excellent fit of the above model to a CO_2 curve deduced from some indirect proxy data (Fig. 66). This fit was obtained before the much more reliable paleo CO_2 ice core data became available, which does not seem at a;; close to the fitted proxy of Fig. 66.
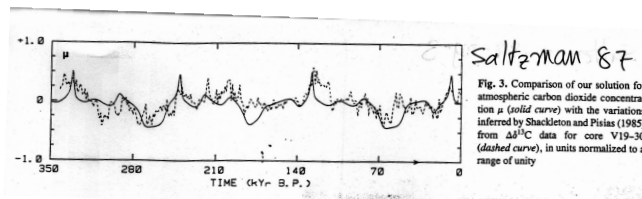

Figure 66: Fit of model results to CO_2 proxy. Fit is quite wonderful, but the proxy data turned out later not to be very accurate... (Fig. 3 from Saltzman [53]).

The parameterization of physical processes is quite vague in these models (e.g. "we are assuming that positive feedbacks due to ice albedo and ice baroclinicity effects, bedrock depression, and sea level changes can roughly balance the dissipative tendencies"... or "the second order nonlinear term $-a_2\mu'^2$ is included to represent the weakening of the climate forcing of ice accumulation as increasing sea ice and cold ocean surface temperatures associated with decreasing μ reduce the sources for snowfall over the ice sheets"). This vagueness often does not allow the model to make specific predictions that may be falsified by observations.

These models do teach us one important lesson: it seems likely that practically any model that has a free (self-sustained) nonlinear oscillation at about 100 kyr period and that is forced by Milankovitch forcing will result

in a good fit to the global ice volume proxy curves, so that these two elements seem a robust part of the glacial puzzle. Saltzman's philosophy was to consider numerous climate feedbacks such that "... a qualitative judgment must be made concerning the dominance of one [feedback] over the other. The ultimate test of the validity of the judgment is the agreement of the output with the observational evidence". This approach and the good fit to observations it yields might have been useful initially, but the next step in understanding the glacial oscillations must be based on a more detailed and specific model that makes specific *falsifiable* predictions that may be tested using the paleo record.

9.9.7   Some additional glacial mechanisms and models

There are quite a few more glacial theories that we shall not describe here, some of which are worth mentioning at least briefly:

1. Thermohaline circulation (as an explanation for ice ages, and/ or for the global scale of the glacial signal). This mechanism is based on the following feedback loop. A stronger THC results in more poleward heat transport, therefore in more melting of land ice. This results in a fresh water input into the oceans which weakens the THC, and so on, leading to an oscillation. Note that the THC is often also mentioned as the source of multiple steady states in the climate system (e.g. [40]); these ideas are more often than not formulated descriptively (Fig. 67) and sometime a bit vaguely rather than using a specific mathematical model for the thermohaline circulation.

2. Some older and/ or just likely wrong ideas for the source of the glacial cycles: Volcanic eruptions, the earth passing through interplanetary dust clouds every 10^5 years; The lost continent of Atlantis ...

3. DMS feedbacks (Charlson, Lovelock et al [7]). Here the feedback loop is as follows: increased temperature $\rightarrow$ more biological productivity $\rightarrow$ more Dimethylsulphide (CCN) $\rightarrow$ more clouds $\rightarrow$ higher albedo $\rightarrow$ lower temperature. etc, again leading to an oscillation. On the other hand DMS feedbacks may act in a different way (Watson and Liss [64]): ice cores seem to show that colder periods have more DMS $\rightarrow$ biology caused additional cooling and therefore helped amplifying the glacial signal.

What Drives Glacial Cycles?

Massive reorganizations of the ocean-atmosphere system, the authors argue, are the key events that link cyclic changes in the earth's orbit to the advance and retreat of ice sheets

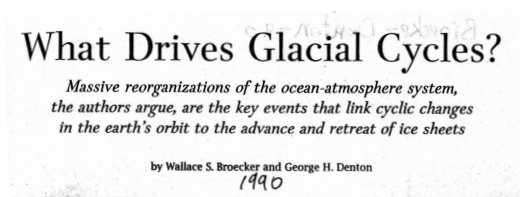by Wallace S. Broecker and George H. Denton
1990

Figure 67: A thermohaline theory for the glacial cycles

9.10 Sea-ice switch mechanism

Gildor and Tziperman [16, 18, 17] proposed that there are three major components that determine the glacial cycle dynamics: land ice, global temperature, and sea ice extent. Their mechanism is based on the temperature-precipitation feedback, modified by the effects of sea ice which acts as a "switch" of the climate system, switching it from glaciation to deglaciation modes. The model used to demonstrate the sea ice switch mechanism was a detailed box model with prognostic sea ice, an 8-box ocean model for the THC temperature and salinity, a prognostic land ice model, and an atmospheric 4-box energy balance model. However, the essence of the mechanism may be described using a far simpler toy model used by [60]. We start by assuming, based on the results of the more detailed model, that the sea ice area is very sensitive to the climate temperature, and jumps from very small area to large area as the temperature decreases below some critical freezing temperature. In the detailed box model mentioned above, the sea ice growth occurs within some 50 years and is accelerated by the sea ice albedo feedback. Note that a similar assumption regarding the dependence of sea ice albedo on the temperature was used for example by [33] as shown in Fig. 57. This assumption allows us to parameterize the sea ice area as function of atmospheric temperature

$$a_{sea-ice} = \begin{cases} \delta I^0_{sea-ice} & T > T_f \\ I^0_{sea-ice} & T < T_f \end{cases} \tag{38}$$

where $I^0_{sea-ice}$ is the maximal sea ice area during a cold period, and $\delta I^0_{sea-ice}$ represents the much smaller sea ice area during warm periods. Snow accumulation over the land glaciers is assumed to depend on both the temperature (temperature-precipitation feedback) and the extent of sea ice (due to its effects on the precipitation over land ice via limiting evaporation from the polar ocean and via the diversion of the storm track, see previous lecture),

$$P(T, a_{sea-ice}) = (P_0 + P_1 \, q(T)) \times \left(1 - \frac{a_{sea-ice}}{a_{ocn}} \right)$$

where a_{ocn} is the ocean area. The humidity $q(T)$ appearing in the last equation is determined by the approximate Clausius-Clapeyron equation

$$q(T) = q_r \, \epsilon_q \, A \, \exp(-B/T)/P_s.$$

The ablation is function of the temperature and of the 41 kyr component of the Milankovitch summer radiation,

$$S_{abl}(T, t) = S_0 + S_M \, \sin(2\pi t/41kyr) + S_T T.$$

The two prognostic model equations may now be written for the land ice mass balance

$$\frac{dV_{land-ice}}{dt} = P(T, a_{sea-ice}) - S_{abl}(T, t)$$

and for the global temperature

$$\frac{dT}{dt} = -\varepsilon \sigma T^4 + H_s (1 - \alpha_s \frac{a_{sea-ice}}{a_{ocn}})(1 - \alpha_L \frac{a_{land-ice}}{a_{land}})(1 - \alpha_C)$$

where the albedos of sea ice, land and clouds are represented by $\alpha_s, \alpha_L, \alpha_C$ respectively. These equations result in a self-sustained 100 kyr oscillations even without the Milankovitch forcing, which are basically the same as the oscillations of the more elaborated box model. Fig. 68 shows the results of the detailed box model with no Milankovitch forcing, which we now use to explain the different stages in the sea ice switch mechanism for the glacial cycles.

- start at $t = 200$ kyr; An interglacial period, warm ocean and atmosphere, no glaciers over land and no sea ice (sea ice switch is "off")
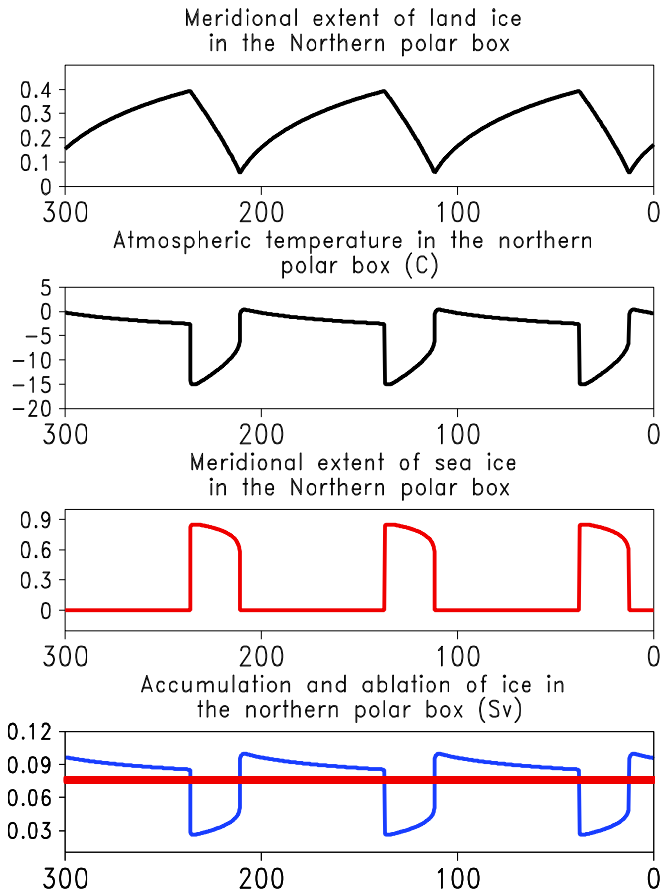
Figure 68: The sea ice switch glacial cycle mechanism. Shown are the results of the box model of [18] as function of time; time is plotted "backward", in units of 10^3 years before "present".

- The warm and therefore moist atmosphere results in a large snow accumulation rate, and the glaciers grow slowly (panel a). Land albedo therefore increases and this results in a slow cooling (panel b). This stage lasts some 70-90 kyr.

- $t = 130$ kyr; The general slow cooling finally causes the upper ocean to cool to the freezing temperature. At this stage a large sea ice cover forms within a few decades, growth being accelerated by the sea ice albedo feedback: once some sea ice is formed, its albedo effect cools the atmosphere, which in turns cools the ocean, leading to the formation of more sea ice. The sea ice growth is also self-limiting: a large sea ice cover insulates the ocean from the cold atmosphere, eventually preventing more cooling of the ocean and more sea ice growth. Sea ice tends to grow at a uniform thickness of some 2-4 meters, rather than grow in thickness. At this time the sea ice switch is "on", panel c; this is the glacial maximum: large glaciers, extensive sea ice, cold atmosphere and ocean.

- The large sea ice area cover results in a cold and therefore dry atmosphere. This implies a low rate of precipitation, so that ablation (melting) of glaciers is larger than accumulation (panel d), and the start of deglaciation.

- $t = 110$ kyr; land glaciers withdraw and land albedo gets smaller. The atmospheric and oceanic temperature therefore increases, until the ocean warms sufficiently and sea ice melts within decades again (switch is "off"). The climate system is back to the initial state, and the cycle starts over.

Bottom line: land glaciers grow during warm periods when there is no sea ice cover, and withdraw during cold period when there is an extensive sea ice cover. Note the hysteresis effect which may be seen by plotting the sea ice extent vs land ice volume throughout the cycle.

9.10.1 Mid-Pleistocene transition from 41 kyr to 100 kyr glacial cycles

Earth's climate has been gradually cooling over the past few millions of years due to gradual CO_2 drop induced by tectonic weathering processes (Fig. 2). This cooling was suggested as a possible source of the change in the character of the glacial oscillations during the Mid-Pleistocene, some 1 Myr ago (Fig. 3), from a 41 kyr oscillation to a 100 kyr oscillation (Maach and Saltzman [34]). An alternative/ complementary explanation has been a hypothesized gradual increase of land ice sheets (Ghil and Childress [15]).

A theory for the glacial cycles should certainly also explain the mid-Pleistocene change in the characteristics of these cycles. Let us consider here a specific mechanisms for the Mid-Pleistocene transition, based on the sea ice switch mechanism. Begin by considering the accumulation of snow over land ice as function of some averaged global atmospheric temperature (Fig. 69).

Note first that due to the temperature-precipitation feedback, a warmer temperature implies a larger precipitation rate, and therefore a larger rate of snow accumulation over land glaciers. This regime is seen to the right of the vertical dash line in the figure. If the temperature is yet warmer (beyond point (a) in Fig. 69), precipitation falls as rain instead of snow, and the rate of accumulation drops. Now, at colder temperatures, extensive sea ice forms at at some critical temperature as the ocean reaches the freezing point, and this reduces the accumulation rate because of the effects of sea ice on the atmospheric temperature, on the storm track, and on limiting evaporation from the polar ocean as discussed above. We have seen that the growth of an extensive sea ice cover occurs at some critical temperature, so it in fact induces a jump in the accumulation rate at that temperature, as seen in the vertical dash line in the figure. Below the temperature at which sea ice forms, the accumulation rate is small and is less sensitive to the temperature changes.

The ablation of land ice is expected to increase with increasing temperature which enhances melting (red dotted line in figure), and we also note again that ablation is also strongly controlled by summer solar radiation (Held [22]).
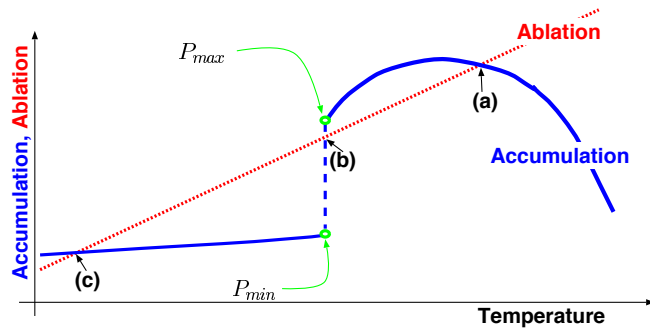
Figure 69: Schematic plot of ablation and accumulation as function of temperature.

Proxy observations indicate a very warm deep ocean a few Myr ago, of the order of 15 degree C. Let us consider, therefore, the effect of the deep ocean temperature on the accumulation - temperature relation (Fig. 70).

A warm deep ocean leads to weaker vertical stratification, and therefore stronger mixing between deep and surface ocean. As a result, the entire ocean, not only the upper ocean, needs to be cooled to create sea ice. Stronger vertical mixing also leads to stronger THC (Bryan, [5]), and therefore to higher polar temperatures. These effects mean that, when deep ocean is warmer, atmospheric temperature needs to be colder before sea ice can form. This amounts to a change in the value of T_f of equation (38). This all means that when the deep ocean is warmer, the vertical dash line representing the jump in accumulation due to the formation of sea ice is further to the left as seen in the upper panel of Fig. 70. This figure is the base for our speculations regarding the Mid-Pleistocene transition.

Consider the climate steady states and their stability based on Fig. 70.

- At points (a,b,c) in the upper panel of Fig. 70, ablation equals accumulation, so that the land glaciers and therefore the climate system is in steady states at these temperatures.

- By considering the effects of small temperature changes on the accumulation and ablation rates, it is easy to see that points (a) and (c) are unstable steady states, leading in the direction of runaway greenhouse and snowball earth scenarios. Suppose, for example, that the climate system is at point (a) and consider a small warm temperature perturbation. The small warming leads according to the figure to a regime in which the ablation is larger than the accumulation, so the glaciers would withdraw. The albedo effect of the withdrawing glaciers leads to further warming, hence a positive feedback that results in an instability that causes the climate to get away from point (a). Similar considerations show that point (c) is also unstable.

- For warm deep ocean (upper panel of Fig. 70), point (b) is a stable steady state. Adding the effect of Milankovitch variations on ablation, results in small, linear, symmetric oscillations around this steady state. This is the proposed mechanism of the 41 kyr glacial variability prior to the Mid-Pleistocene. Admittedly this does not explain why the oscillations prior to the bifurcation point are of a period of 41 kyr and not 19 or 23 kyr, and this would have to wait for further work.

- For cold deep ocean, point (b) is no longer on the accumulation curve in the lower panel of Fig. 70, because it lies on the sea-ice induced jump in accumulation. This is the regime in which the sea ice switch 100 kyr glacial oscillations occur, as described in the following section.

So, a deep ocean cooling induces a transition from symmetric 41 kyr oscillation to asymmetric nonlinear 100 kyr oscillation. This is due to a bifurcation of the climate system due to the change in the accumulation temperature

128

relation as described above. That this is a bifurcation means that there is a threshold that the deep ocean cooling crosses in order to have the system cross the bifurcation point (that is, make point (b) lie on the vertical dash line). This is the proposed mechanism for the observed climate shift of 1 Myr ago [60]. Note that since the deep water cooling needs to cross a certain threshold to activate the sea ice switch oscillations, it does not matter when most of the deep ocean cooling has occurred (presumably more than a few million years ago), but only when the threshold was crossed by T_f in equation (38) (which we speculate has happened one Myr ago).
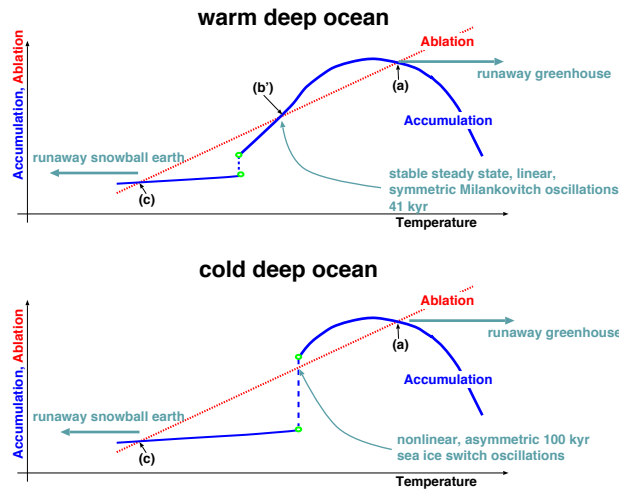

Figure 70: Ablation and accumulation as function of temperature, for warm and for cold deep ocean states.

Making T_f in (38) a slowly varying function, decreasing with time, and integrating the above simple model of the sea ice switch mechanism, we obtain the results in Fig. 71, showing a Mid-Pleistocene like transition from small amplitude 41 kyr oscillations to larger amplitude 100 kyr glacial oscillations. It would certainly be interesting to perform a more careful bifurcation analysis to find out precisely what kind of a bifurcation the Mid-Pleistocene transition corresponds to in this model. . .

129

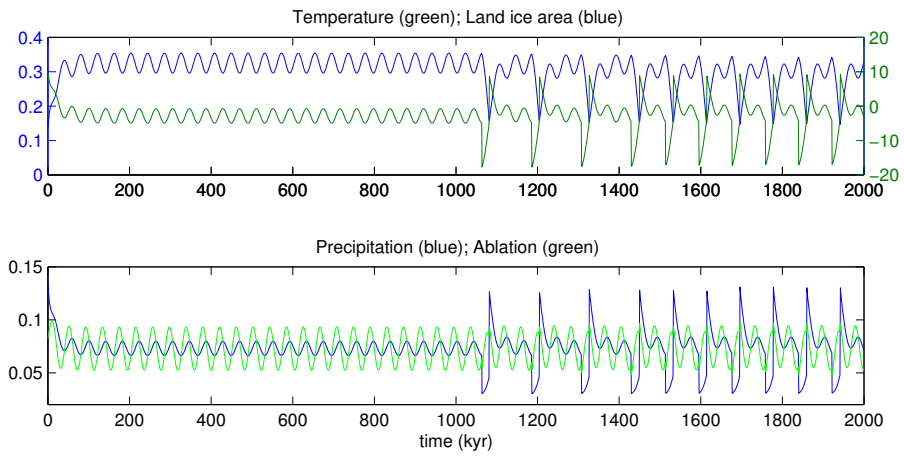Figure 71: A simulation of the mid-Pleistocene transition from [60].

9.11 Biogeochemical toy models for glacial CO2 variability

Given the clear signal of glacial-interglacial CO_2 changes (Fig. 37), it is natural to wonder if CO_2 variations cause the glacial cycles via their greenhouse effect. Alternatively, could the CO_2 variations have been caused by the glacial cycle in the physical climate system so that they only served to amplify the glacial variability? We only discuss here the possibility that CO_2 variations are driven by the glacial cycles rather than being an essential element for the existence of these cycles. We therefore need to explain how the CO_2 variations are caused. As a background material, the reader is referred to the various geochemical textbooks for a review of some of the relevant feedbacks and issues [63], including the following terms.

1. Soft tissue pump (reduces atmospheric CO_2).

2. Hard tissue pump (increases atmospheric CO_2 due to Alkalinity effects).

3. Solubility pump: increased atmospheric CO_2 when the ocean warms.

4. Redfield ratio: **106 C : 16 N : 1 P**.

5. Productivity (and its dependence on light and nutrients), export production.

6. Iron fertilization (possible increase in biological productivity in high latitudes during the last glacial maximum; effects of increased dust levels etc.

7. CO_2 gas exchange between ocean and atmosphere; dominance of oceanic carbon reservoir, and especially of the deep ocean reservoir.

9.11.1 Atmospheric CO_2 and vertical ocean mixing

Toggweiler [57] has used a variety of box models, starting with the simplest 3 box model (Fig. 72) to propose a geochemical mechanism for the glacial changes in atmospheric CO_2.
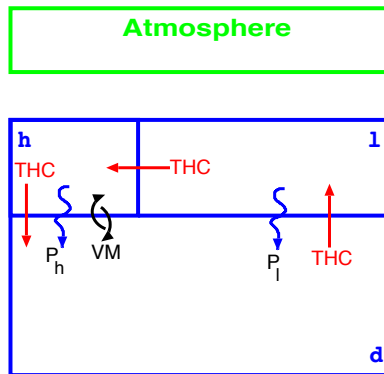

Figure 72: A box model for glacial-interglacial CO_2 variations. The boxes represent the upper mid-latitude ocean (l), the surface polar ocean (h) and the deep ocean (d), as well as the atmosphere.

In the box model of Fig. 72, one may write the (total) carbon ΣCO_2 balance for the deep box under steady-state conditions as a balance of advection (by the thermocline circulation THC) and mixing (by VM, via some

internal wave mechanism), plus a term that represents the sinking of carbon from the surface boxes to the deep box as part of the export production from the low and high latitude surface boxes $P_l + P_h$:

$$0 = (VM_{hd} + THC) * (\sum CO_{2h} - \sum CO_{2d}) + Red_{C:P}(P_l + P_h),$$

where $Red_{C:P}$ is the Redfield Ratio. Assume $P_l = THC * PO_{4d}$, which means that we assume all the surface nutrients in the mid-latitude box to be utilized by the biological activity and be converted to export production. Further assume $P_l \gg P_h$ meaning again that the mid-latitude biological activity is very efficient, acts over a larger area relative to that of the high latitudes, and therefore utilizes all the available nutrients. Using these assumptions we have

$$\sum CO_{2d} - \sum CO_{2h} = Red_{C:P} \frac{THC * PO_{4d}}{VM_{hd} + THC}.$$

For a sufficiently fast gas exchange with the atmosphere, upper ocean $\sum CO_2$ in lower and higher latitudes are equal, so that

$$\sum CO_{2d} - \sum CO_{2l} \sim Red_{C:P} \frac{THC * PO_{4d}}{VM_{hd} + THC}, \tag{39}$$

which is the result we were after: the $\sum CO_2$ difference between the upper and deep ocean is controlled by vertical mixing and by the amplitude of the THC. A reduction in vertical mixing in the high latitude Southern Ocean should result according to (39) in an increase of the concentration of (total) carbon difference between the upper and deep ocean. Taking the deep ocean concentration to be constant due to its large reservoir, this implies a reduction of the surface total carbon and CO_2 concentration. Since the atmospheric CO_2 concentration is determined by that of the upper ocean, we can expect that a reduction of the vertical mixing in the Southern Ocean would lead to a reduction in atmospheric CO_2 [57]. However, this mechanism is not capable of explaining why the vertical mixing in the ocean should change, and this is what we do in the following section based on the sea ice switch mechanism again.

9.11.2 Sea ice switch and mechanism of vertical mixing change in the Southern Ocean

The biochemistry mechanism of Toggweiler [57] described in the above section specifies a change in the vertical mixing between the deep and the surface Southern Ocean. However, no physical mechanism is provided for this change in the physical climate system. A physical mechanism for the vertical mixing changes that may result in the glacial-interglacial CO_2 variations was proposed by Gildor and Tziperman [17], based on the sea ice switch mechanism, as follows. The stratification in the Southern Ocean (SO) is composed of cold, fresh and therefore light water above warm, salty and therefore dense water. Glacial conditions in the northern hemisphere cool the North Atlantic Deep Water (NADW), and consequently, via the southward flow of NADW, cool the deep temperature in the SO. Because of the permanent ice cover over Antarctica, the surface ocean temperature in the SO near Antarctica is close to the freezing point during the entire glacial cycle, so that it cannot cool very much even during glacial conditions in the northern hemisphere. Glacial conditions therefore increase the density of deep SO water but not of the surface SO water. This strengthens the vertical stratification in the SO. As a result, vertical mixing in the SO is expected to be reduced, based on a simple internal wave parameterization for the vertical mixing coefficient such as $\kappa_v \propto \left(\frac{\partial \rho}{\partial z}\right)^{-\alpha}$ (Gargett [13]). Thus we have explained the vertical mixing change in the Southern ocean as being a result of the northern hemisphere glaciation, and hence provided the missing link between the atmospheric CO_2 variations induced by the biogeochemistry and between the physical climate system.

Note that this mechanism implies that the northern hemisphere leads the southern hemisphere during the glacial cycles, and that temperature changes in the northern hemisphere lead CO_2 changes in the southern hemisphere. The time lag between the two hemispheres, and in particular between temperature northern hemisphere

temperature and atmospheric CO_2, is expected to be the time it takes the cooling signal to propagate from the northern hemisphere to the southern hemisphere, via the advection of the NADW. This is roughly a time scale of 500-1500 years. The phase relation between the two hemisphere seems to still be under debate in the paleo literature.

References

[1] P. Bak, T. Bohr, and M. H. Jensen. Mode-locking and the transition to chaos in dissipative systems. *Physica Scripta*, T9:50–58, 1985.

[2] D. S. Battisti. The dynamics and thermodynamics of a warming event in a coupled tropical atmosphere/ocean model. *J. Atmos. Sci.*, 45:2889–2919, 1988.

[3] R. Benzi, G. Parisi, A. Sutera, and A. Vulpiani. Stochastic resonance in climatic change. *Tellus*, 34:10–16, 1982.

[4] W. S. Broecker. *The glacial world according to Wally*. Eldigio Press, 1995.

[5] F. Bryan. Parameter sensitivity of primitive equation ocean general circulation models. *J. Phys. Oceanogr.*, 17:970–985, 1987.

[6] N. Calder. Arithmetic of ice ages,. *Nature,*, 252:216–218, 1974.

[7] R. J. Charlson, J. E. Lovelock, M. O. Andreae, and S. G. Warren. Oceanic phytoplankton, atmopsheric sulphur, cloud albedo and climate. *Nature*, 326:655–661, 1987.

[8] K.M. Cuffey and G.D. Clow. Temperature, accumulation, and ice sheet elevation in central Greenland through the last deglacial transition. *J. Geophys. Res.*, 102:26,383–26,396, 1997.

[9] H. A. Dijkstra. *Nonlinear physical oceanography*. Kluwer Academic Publishers, 2000.

[10] B. F. Farrell and P. J. Ioannou. Generalized stability theory part I: autonomous operators. *J. Atmos. Sci.*, 53:2025–2040, 1996.

[11] Brian Farrell. Optimal excitation of neutral Rossby waves. *J. Atmos. Sci.*, 45:163–172, 1988.

[12] E. Galanti and E. Tziperman. ENSO's phase locking to the seasonal cycle in the fast SST, fast wave, and mixed mode regimes. *J. Atmos. Sci.*, 57:2936–2950, 2000.

[13] A.E. Gargett. Vertical eddy diffusivity in the ocean interior. *J. Mar. Res.*, 42:359–393, 1984.

[14] M. Ghil. Cryothermodynamics: the chaotic dynamics of paleoclimate. *Physica D*, 77:130–159, 1994.

[15] M. Ghil and S. Childress. *Topics in Geophysical Fluid Dynamics: Atmospheric Dynamics, Dynamo Theory and Climate Dynamics*. Springer-Verlag, New York, 1987.

[16] H. Gildor and E. Tziperman. Sea ice as the glacial cycles climate switch: role of seasonal and orbital forcing. *Paleoceanography*, 15:605–615, 2000.

[17] H. Gildor and E. Tziperman. Physical mechanisms behind biogeochemical glacial-interglacial CO_2 variations. *Geophys. Res. Lett.*, 28:2421–2424, 2001.

[18] H. Gildor and E. Tziperman. A sea-ice climate-switch mechanism for the 100 kyr glacial cycles. *J. Geophys. Res.*, 106(C5):9117–9133, 2001.

[19] A. E Gill. Some simple solutions for heat-induced tropical circulation. *Q. J. R. Meteorol. Soc.*, 106:447–462, 1980.

[20] Adrian E. Gill. *Atmosphere-Ocean Dynamics*. Academic Press, Inc, San Diego, CA, 662pp, 1982.

[21] Z. Hao, J. D. Neelin, and F.F. Jin. Nonlinear air-sea interaction in the fast-wave limit. *J. Climate*, 6:1523–1544, 1993.

[22] I.M. Held. Climate models and the astoromical theory of ice age. *Icarus*, 50:449–461, 1982.

[23] A. C. Hirst. Unstable and damped equatorial modes in simple coupled ocean-atmosphere models. *J. Atmos. Sci.*, 43:606–630, 1986.

[24] T. J. Hughes. *Ice sheets*. Oxford University Press, 1998.

[25] P. Huybrechts and J. Oerlemans. Response of the Antarctic ice sheet to future greenhouse warming. *Clim. Dyn.*, 5:93–102, 1990.

[26] J. Imbrie and J. Z. Imbrie. modelling the climatic response to orbital variations. *Science*, 207:943–953, 1980.

[27] F.-F. Jin. An equatorial ocean recharge paradigm for ENSO. Part I: conceptual model. *J. Atmos. Sci.*, 54:811–829, 1997.

[28] F.-F. Jin. An equatorial ocean recharge paradigm for ENSO. Part II: a stripped-down coupled model. *J. Atmos. Sci.*, 54:830–847, 1997.

[29] F.-F. Jin and D. Neelin. Modes of interannual tropical ocean-atmosphere interaction - a unified view. Part I: numerical results. *J. Atmos. Sci.*, 50:3477–3503, 1993.

[30] F.-F. Jin and D. Neelin. Modes of interannual tropical ocean-atmosphere interaction - a unified view. Part III: analytical results in fully coupled cases. *J. Atmos. Sci.*, 50:3523–3540, 1993.

[31] F-F Jin, D. Neelin, and M. Ghil. ENSO on the devil's staircase. *Science*, 264:70–72, 1994.

[32] R. Kleeman and A. M. Moore. A theory for the limitation of ENSO predictability due to stochastic atmospheric transients. *J. Atmos. Sci.*, 54:753–767, 1997.

[33] H. Le-Treut and M. Ghil. Orbital forcing, climatic interactions, and glaciations cycles. *J. Geophys. Res.*, 88:5167–5190, 1983.

[34] K.A. Maasch and B. Saltzman. A low-order dynamical model of global climatic variability over the full Pleistocene. *J. Geophys. Res.*, 95:1955–1963, 1990.

[35] G.H. Miller and A. de Vernal. Will greenhouse warming lead to Northern Hemisphere ice-sheet growth? *Nature*, 355:244–246, 1992.

[36] M. Munnich, M. A. Cane, and S. E. Zebiak. A study of self-excited oscillations of the tropical ocean-atmosphere system. *J. Atmos. Sci.*, 48:1238–1248, 1991.

[37] J. D. Neelin. The slow sea surface temperature mode and the fast-wave limit: analytic theory for tropical interannual oscillations and and experiments in a hybrid coupled model. *J. Atmos. Sci.*, 48:584–605, 1991.

[38] J. D. Neelin and F.-F. Jin. Modes of interannual tropical ocean-atmosphere interaction - a unified view. part ii: analytical results in the weak-coupling limit. *J. Atmos. Sci.*, 50:3504–3522, 1993.

[39] J. Oerlemans. Some basic experiments with a vertically integrated ice sheet model. *Tellus*, 33:1–11, 1981.

[40] D Paillard. The timing of Pleistocene glaciations from a simple multiple-state climate model. *Nature*, 391:378–381, 1998.

[41] D. Paillard. Glacial cycles: toward a new paradigm. *Rev. Geophys.*, 39:325–346, 2001.

[42] W.S.B. Paterson. *The Physics of Glaciers*. Pergamon, 3rd edition, 1994.

[43] J. Pedlosky. *Geophysical Fluid Dynamics*. Springer-Verlag, Berlin-Heidelberg-New York., 2 edition, 1987.

[44] W.R. Peltier and S. Marshall. Coupled energy-balance/ice-sheet model simulations of the glacial cycles: a possible connection between terminations and terrigenous dust. *J. Geophys. Res.*, 100:14,269–14,289, 1995.

[45] C. Penland and P. D. Sardeshmukh. The optimal-growth of tropical sea-surface temperature anomalies. *J. Climate*, 8(8):1999–2024, August 1995.

[46] S. G. Philander. El Niño southern oscillation phenomena. *Nature*, 302:295–301, 1983.

[47] S. G. H. Philander. *El Niño, La Niña, and the Southern Oscillation*. Academic Press, San Diego, 1990.

[48] D. Pollard. A simple ice sheet model yields realistic 100 kyr glacial cycles. *Nature*, 296:334–338, 1982.

[49] D Pollard. A coupled climate-ice sheet model applied to the Quaternary ice ages. *J. Geophys. Res.*, 88:7705–7718, 1983.

[50] D. Pollard. Ice-age simulations with a calving ice-sheet model. *Quat. Res.*, 20:30–48, 1983.

[51] J. A. Rial. Pacemaking the ice ages by frequency modulation of earth's orbital eccentricity. *Science*, 285(5427):564–568, jul 23 1999.

[52] B. Saltzman and A. Sutera. A model of the internal feedback system involved in Late Quaternary climatic variations. *J. Atmos. Sci.*, 41:736–745, 1984.

[53] Barry Saltzman. Carbon dioxide and the $\delta^{18}O$ record of late-Quaternary climatic change: a global model. *Clim. Dyn.*, 1:77–85, 1987.

[54] H. G. Schuster. *Deterministic Chaos*. VCH, 2nd edition, 1989.

[55] H. Stommel. Thermohaline convection with two stable regimes of flow. *Tellus*, 13:224–230, 1961.

[56] M. J. Suarez and P. S. Schopf. A delayed action oscillator for ENSO. *J. Atmos. Sci.*, 45:3283–7, 1988.

[57] J. R. Toggweiler. Variation of atmospheric CO_2 by ventilation of the ocean's deepest water. *Paleoceanography*, 14:572–588, 1999.

[58] E. Tziperman, M. A. Cane, and S. E. Zebiak. Irregularity and locking to the seasonal cycle in an ENSO prediction model as explained by the quasi-periodicity route to chaos. *J. Atmos. Sci.*, 52(3):293–306, feb 1 1995.

[59] E. Tziperman, M. A. Cane, S. E. Zebiak, Y. Xue, and B. Blumenthal. Locking of El Nino's peak time to the end of the calendar year in the delayed oscillator picture of ENSO. *J. Climate*, 11(9):2191–2199, September 1998.

[60] E. Tziperman and H. Gildor. The mid-Pleistocene climate transition and the source of asymmetry between glaciation and deglaciation times. *Paleoceanography*, 18(1):10.1029/ 2001PA000627, 2003.

[61] E. Tziperman, L. Stone, M. A. Cane, and H. Jarosh. El-Nino chaos: overlapping of resonances between the seasonal cycle and the Pacific ocean-atmosphere oscillator. *Science*, 264(5155):72–74, apr 1 1994.

[62] E. Tziperman, S. E. Zebiak, and M. A. Cane. Mechanisms of seasonal - ENSO interaction. *J. Atmos. Sci.*, 54(1):61–71, jan 1 1997.

[63] T. Volk and M.I. Hoffert. Ocean carbon pumps: analysis of relative strengths and efficiencies in ocean-driven atmospheric CO_2 changes. In E. T. Sundquist and W. S. Broecker, editors, *The carbon cycle and atmospheric CO_2: natural variations Archean to present*, volume 32 of *Geophysical monograph*, pages 99–110. American Geophysical Union, 1985.

[64] A. J. Watson and P. S. Liss. Marine biological controls on climate via the carbon and sulphur geochemical cycles. *Phil. Trans. R. Soc. Lond. B*, 353:41–51, 1998.

[65] R.G. Watts and E. Hayder. A two-dimensional, seasonal, energy balance climate model with continents and ice sheets: testing the Milankovitch theory. *Tellus*, 36:120–131, 1984.

[66] S. E. Zebiak and M. A. Cane. A model El Niño-Southern Oscillation. *Mon. Weath. Rev.*, 115:2262–2278, 1987.